Atomically precise impurity identification and modification on the manganese doped GaAs(110) surface with scanning tunneling microscopy

J. K. Garleff,[1,*] C. Çelebi,[1] W. Van Roy,[2] J.-M. Tang,[3] M. E. Flatté,[4] and P. M. Koenraad[1]

[1]*COBRA Inter-University Research Institute, Department of Applied Physics, Eindhoven University of Technology, P.O. Box 513, NL-5600 MB Eindhoven, The Netherlands*

[2]*IMEC, Kapeldreef 75, B-3001 Leuven, Belgium*

[3]*Department of Physics, University of New Hampshire, Durham, New Hampshire 03824, USA*

[4]*Optical Science and Technology Center and Department of Physics and Astronomy, University of Iowa, Iowa City, Iowa 52242, USA*

(Received 31 January 2008; revised manuscript received 9 April 2008; published 14 August 2008)

Cross-sectional scanning tunneling microscopy (STM) measurements on molecular beam epitaxy grown Mn doped GaAs(110) at 5 and 77 K are presented. The enhanced mechanical stability of the STM at low temperature allows a detailed study of the electronic contrast of Mn atoms in the GaAs(110) surface. According to reproducible and distinguishable contrast patterns of single Mn atoms, we present statistical evidence for a layer by layer identification of Mn atoms embedded in the first few monatomic layers of the crystal. A comparison with a bulklike theoretical approach reveals a *semiquantitative* agreement with the measurements. Remaining differences between theory and experiment indicate the influence of the surface as an important factor to understand the contrast of impurities close to the surface. Furthermore, we report the injection of transition-metal atoms into the surface. Finally, reproducible complexes consisting of a surface Mn and an adsorbate atom are found and manipulated.

DOI: 10.1103/PhysRevB.78.075313 PACS number(s): 68.37.Ef, 68.47.Fg, 73.20.At

I. INTRODUCTION

The investigation of individual isolated impurities has gained increasing scientific interest since the invention of scanning tunneling microscopy (STM) by Binnig *et al.*[1,2] Due to the technical importance of impurities in optoelectronic devices with ever decreasing sizes, individual shallow dopants in semiconductors such as Si and GaAs have been investigated. Examples are phosphorus[3] and boron in silicon,[4] beryllium, carbon, and zinc[5,6] as shallow acceptors in GaAs and silicon (Si_{Ga}) (Ref. 7) as a shallow donor in GaAs. Observation of the magnetic properties of Mn in III-V semiconductors[8–10] led to increased interest in this high-binding-energy acceptor. STM images of isolated Mn in GaAs were published in 2004,[11] followed by images of pairs of Mn atoms[12] and Mn atoms in strained environments.[13] Whereas these experiments were performed on Mn doped samples, another group used the STM as a tool to insert Mn atoms[14] into the first layer of GaAs(110) and to explore their properties. When investigating impurities close to a surface, one has to consider the surface-induced modification of the lattice. For the Si(111) surface, the 2×1 reconstruction was found[15,16] to dominate the observed contrast of P atoms in the first few layers of the crystal. The experiments on Mn in GaAs mentioned above, however, have been interpreted on the basis of bulk properties and theoretical models neglecting the surface because the relaxation on GaAs(110) is expected to have only a minor effect on the electronic properties. Nevertheless, the broken symmetry at the surface substantially modifies the binding energy of the Si_{Ga} donor close to the GaAs(110) surface.[17] The wave function of other dopant atoms therefore can be supposed to be modified by the surface when observed by STM. General trends of Mn atoms close to GaAs surface were observed by STM and have been reported to be correctly predicted by basically bulklike theory. Surprisingly this was even reported for the STM results of Mn atoms located directly in the first layer of GaAs(110).[14]

Since the expected modifications should depend on the substitutional depth of the impurity below the surface, the exact position of the addressed atomic defect is of crucial interest to understand the details of the observed contrasts. An earlier study of deeply buried acceptors at room temperature (RT) (Ref. 11) estimated the relative depth of individual acceptors using the convincing assumption that the topographic contrast is expected to smear out with increasing depth of the impurity. A second aspect is related to the position of the impurity contrast with respect to the voltage dependent atomic corrugation of the GaAs(110) surface, which allows one to conclude if the defect is substituted in an odd or an even layer below the surface.[18] For Mn in GaAs(110) this approach has been taken in Ref. 19 and will be applied to determine the depth of deeply buried Mn atoms in GaAs in a separate paper.[20] A main difficulty of this method to determine the impurities' depth is the lack of an absolute point to start counting. Mn in the topmost layer is well known and should thus provide a well-defined starting point as a reference. Due to rather strong modifications, which the contrast pattern undergoes if the defect is located close to the surface, e.g., in layer 2, 3, or 4, it has been an open issue how to connect the two regions—"top layer"[14] and "deeply buried."[11] This question is of scientific interest as it was shown recently by comparing STM measurements and *ab initio* calculations that it was possible to identify *P* atoms on the nonequivalent lattice sites of the Si(111)-2×1 surface.[16] Furthermore, detailed knowledge about the substitutional position of an impurity is necessary to interpret spectroscopic or other properties of the impurities which might depend on their depth below the surface. Therefore it will be necessary to know exactly where the defect is located below the surface.

II. EXPERIMENTAL SETUP

To tackle these questions we investigated Mn doped GaAs in an Omicron low-temperature (LT)-STM in UHV conditions (base pressure better than 1×10^{-11} mbar) with cross sectional scanning tunneling microscopy (X-STM). The samples were grown on the (100) surface of a p^+-doped GaAs wafer. The structure consists first of a 70 nm buffer layer of intrinsic GaAs, then 100 nm Mn:GaAs, then 40 nm Mn:AlAs as a marker layer, and 150 nm Mn:GaAs on top. The doping level of 5×10^{18} cm^{-3} was the same for all Mn doped layers, GaAs, as well as AlAs. The samples were cleaved at RT in the UHV chamber to expose a nearly adsorbate-free (110) surface with atomically flat terraces of hundreds of nanometers up to several microns between adjacent atomic step edges.[21] We used electrochemically etched polycrystalline tungsten (W) tips. To achieve sharp tips with high stability, we glowed the tips in UHV (base pressure better than 5×10^{-10} mbar) and bombarded them with Ar^+ ions. Finally the tip preparation was checked by means of field emission of the tip against a half sphere electrode. A low onset voltage of the field-emission current made sure that the tip has a small apex radius. Smooth and reproducible $I(V)$ characteristics of the emission current prove that the tip apex is stable and free of loosely bound adsorbates. The tips were transferred to the STM without breaking the UHV to avoid contamination after UHV preparation. This procedure produces a high percentage of tips that achieve atomic resolution laterally and at the same time good spectroscopic behavior (resolution and long term stability).[22] The sample was inserted into the precooled cryostat within a few minutes of cleavage. After a few hours, when thermal equilibrium was reached, we started the measurements. As usual for X-STM we first had to find the AlAs marker to make sure that we would scan the Mn doped layers. Then the Mn acceptors were identified by their well-known topographic contrast at around +1.5 V.[11] The exact voltage needed to address the Mn atoms depends on the microscopic configuration as well as the chemical composition of the tip apex (which sets the work function[23,24] of the tip). The voltage at which a specific contrast (e.g., the bow tie of a Mn atom) is addressed can thus differ by several hundred millivolts between individual atomic tip configurations.

III. EXPERIMENTAL RESULTS

Two examples of STM topography images recorded in constant current mode are shown in Fig. 1. (See, also, Fig. 2.) As expected for the high doping level a large number of Mn-like features were found. In addition to the well-known contrast of Mn atoms in the first layer[14] of the surface [marked (a) in Fig. 1] and deeply buried Mn acceptors[11] [marked (e) and (f) here], several more patterns appear in our images. Two of them, marked (c) and (d) in Fig. 1, strongly resemble the contrast of deeply buried Mn atoms, whereas the feature marked (b) is completely different to our knowledge. Furthermore we find two defects, marked "P_1" and "P_2" shown in more detail in images I and III in Fig. 3, which roughly resemble the patterns of surface Mn atoms. By comparison with the results from Ref. 14 reproduced in images II and IV in Fig. 3, it is reasonable to assign them to pairs of Mn atoms in the surface layer. P_1 is the nearest-neighbor pair on the Ga sublattice in the $[1\bar{1}0]$ direction, and P_2 is the next-nearest neighbor on the Ga sublattice in the

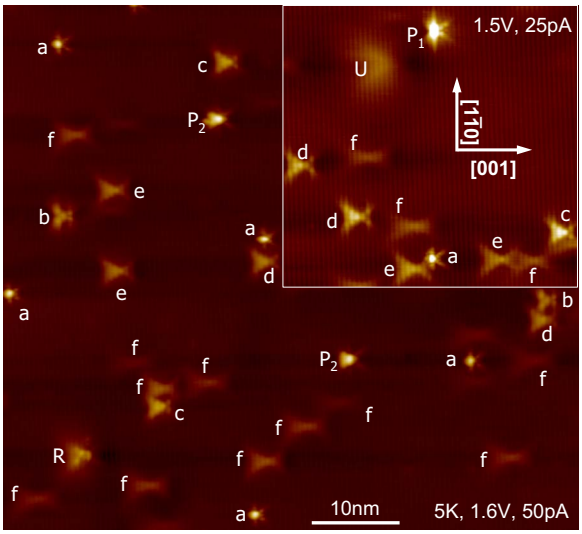

FIG. 1. (Color online) STM topography of Mn:GaAs(110) with defect contrasts. Mn acceptors in the top layer are marked (a). Indices (b)–(e) indicate Mn atoms in the following four layers below the surface. Contrast (f) sums up all deeper buried Mn atoms, P_1 and P_2 are Mn pairs, and U and R are unintended defects, respectively. The crystallographic directions given here are also used for the subsequent figures in this paper.

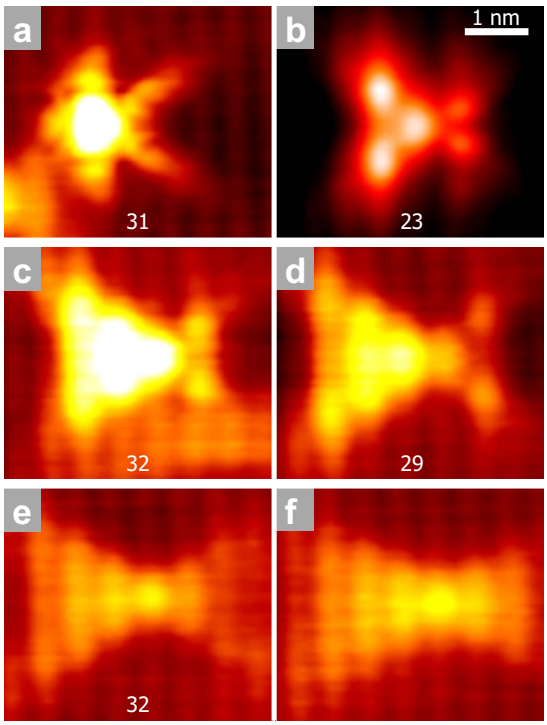

FIG. 2. (Color online) STM topography images of different classes of the contrast of Mn acceptors in GaAs(110). The number beneath each contrast represents how often it appeared in the measurements. Indices (a)–(f) here correspond to those shown in Fig. 1.

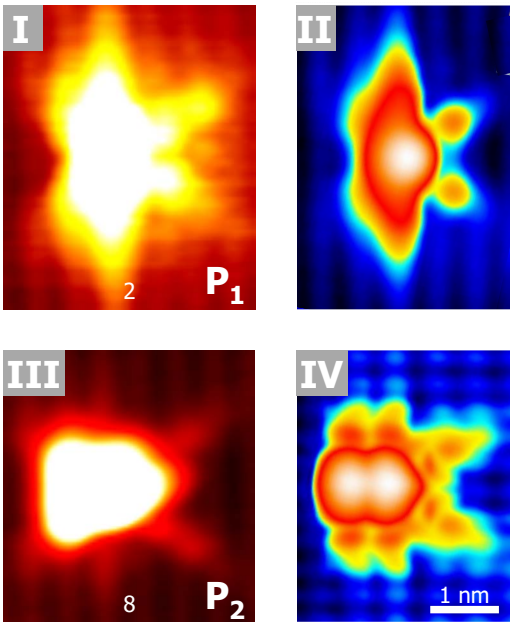

FIG. 3. (Color online) Images I and III: STM topography images zoomed in on patterns P_1 and P_2. Images II and IV: LDOS maps taken from Ref. 14 at $V_{gap}=+1.55$ V on Mn pairs in the topmost layer of GaAs(110). Image II shows a pair of nearest-neighbor Mn atoms in the (110) direction on the Ga sublattice, whereas IV shows a pair of next-nearest neighbors in the (001) direction on the Ga sublattice.

[001] direction. The difference between feature P_2 in our data and the respective contrast in Ref. 14 will be addressed later on in the paper. Finally a large but blurry triangle is marked "U" in the image. It is assigned to an unintended shallow acceptor, probably C or Be (see Ref. 6), and might stem from the background pressure of the molecular beam epitaxy (MBE) chamber. The other unintended defect "R" most probably stems from contamination due to the residual gas in the UHV chamber. To check which of the above described features R, U, P_1, P_2, and (a)–(f) are significant, we improved statistics by the analysis of a large number of images with a total of 147 individual defects distributed between patterns (a)–(e). We were able to confirm the following typical, distinct patterns, which are shown in Fig. 2. All structures listed below have a symmetry axis parallel to the [001] direction. (a) A single Mn atom located in the topmost layer of the surface as described in Ref. 14. (b) Two strong protrusions with a distance of ~1.25 nm along one atomic row in the $[1\bar{1}0]$ direction together with a third protrusion of similar height on the next atomic row in the [001] direction form an isosceles triangle. Two additional smaller and shallower protrusions are located in front of the triangle's head with a distance of ~6.5 Å between them. (c) An isosceles triangle with a height of three atomic rows and a base length of ~1.7 nm with two weak protrusions on both sides in front of its head in the [001] direction, ~1 nm apart. (d) An isosceles triangle with a height of four atomic rows and a base length of ~2.1 nm with two weak protrusions on both sides in front of its head including a distance of ~1.4 nm between them. The middle of the triangle's base is now less protruded than the edges. (e) The isosceles triangle spreads now further than four atomic rows in the [001] direction and evolves thus toward the $[00\bar{1}]$ oriented wing of the well-known bow-tie-shaped contrast of buried Mn acceptors.[11] The two weak protrusions are no longer clearly apart from each other and thus start forming the [001] oriented wing of this pattern, which here only spreads over two atomic rows. (f) The well-known bow-tie pattern of a deeply buried Mn acceptor.[11] The asymmetry between the wings in the [001] and the $[00\bar{1}]$ directions decreases with increasing depth of the impurity below the surface.[20] Thus image (f) stands for a larger group of patterns. Because they are all quite similar to each other we do not investigate them here in more detail.

TABLE I. Number of counts for the different Mn patterns.

Pattern	(a)	(b)	(c)	(d)	(e)	P_1	P_2
Counts	31	23	32	29	32	2	8

We identified and counted the five different patterns (a)–(e) as well as P_1 and P_2 in the measurements. The number of counts for each pattern is displayed in Table I. We also checked patterns (a)–(f) with scanning tunneling spectroscopy. The observation of highly comparable local density of states (LDOS) structure for patterns (a)–(f) confirms our conclusion that they originate from Mn impurities.

In addition there are many more Mn atoms of type (f). As group (f) does not consist of exactly one type of identical contrasts [as groups (a)–(e)], we did not count them in detail. A rough estimate using a smaller population turns out that type (f) shows up to approximately five times more often than each of patterns (a)–(e). If the population of 147 impurities identified as one of the types [(a)–(e)] equally divides into these five patterns, the average count equals 29.4 with a standard deviation, σ, of 5.4. The counts for all defects are thus found within a little more than one σ around the expectation confirming that these patterns have the same density. In addition we know that pattern (a) stems from a Mn atom in the topmost atomic layer on the surface and represents thus the number of Mn atoms within exactly 1 ML (monolayer). We assume a random distribution of the Mn atoms in the MBE grown material. A second prerequisite to interpret our statistics is the fact that the cleavage surface preserves the surface configuration far from thermal equilibrium that is created when the crack travels through the crystal.[25] As the scanned surface is not evolving toward the equilibrium configuration on the time scale of our experiments, no significant diffusion or intermixing takes place. We can thus expect that the Mn acceptors are still randomly distributed. This implies that the probability to find a Mn atom should be equal for all layers in and below the cleavage surface. Since the counts for patterns (b)–(e) are the same as for (a) we conclude that each pattern represents a Mn atom substituted in one specific layer below the surface. To assign each pattern to a specific depth, we take two assumptions: first, the contrast of Mn atoms in GaAs undergoes a smooth transition between the well-known pattern for Mn atoms in the top layer toward deeply buried ones; second, the contrast smears out to a broader but shallower feature with increasing depth

of the buried Mn atom. With these assumptions we can unambiguously assign patterns (b)–(e) to Mn atoms embedded layers 1–4 below the surface (which is equal to layers 2–5 of the crystal).

Let us now return to the result that there are approximately five times as many feature (f) as the average of (a)–(e) yields. Based on each pattern (a)–(e) representing Mn atoms in one atomic layer, feature (f) adds Mn atoms in five more atomic layers since the dopant atoms are statistically distributed over all layers. In our experiments we find that buried Mn atoms are visible in the first ten layers of the crystal surface. This agrees with the depth limit for impurities in a highly doped material to be typically visible in STM and therefore confirms our identification of one layer to each of the patterns (a)–(e). The assignment of features (a)–(e) to Mn atoms in layers 0–4 is confirmed by the changing odd-even mirror symmetry of the contrast with respect to the Ga and the As sublattices and the $(1\bar{1}0)$ mirror plane. This is discussed in more detail in Ref. 20.

IV. INTERPRETATION

Up to now the depth of the Mn atoms has been identified purely based on experimental measurements and basic arguments of geometry and statistics. The independence of our conclusions of any involved theoretical calculation opens up the possibility to compare the results of both approaches. Unfortunately, the existing theoretical "first-principles" density-functional theory (DFT) calculations[26,27] are not useful for studying STM images of Mn defects in GaAs close to the (110) surface. Other simulations are based on tight-binding and effective-mass (EM) methods and both neglect the influence of the surface. So we do not expect full agreement between theory and STM work and rather look for general trends that might be reproduced both in experiment and theory. Figure 4 (Ref. 14, supplementary information) shows simulated STM topography images at a tunneling voltage of +1.55 V of Mn atoms in the first six layers of GaAs(110). As described in this paper, the experimental STM contrast of Mn atoms embedded in layers 2, 3, and 4 of the crystal [patterns (b)–(d)] is mainly characterized as an isosceles triangle with its base perpendicular to the $[00\bar{1}]$ direction and two additional weak protrusions at its apex. The triangle spreads over two, three, or four atomic rows with increasing depth of the Mn atom. If we now focus on the size of the contrast in the [001] direction predicted by theory, we find a nice agreement: except for the weak protrusions in the [001] direction, the number of the enhanced atomic rows in Fig. 4 [images (b)–(d)] is the same as for the respective experimental results [images (b)–(d) in Fig. 2]. The electronic impact of a Mn atom spreads over one additional atomic row for each monolayer the impurity is located more deeply below the surface. The theoretical prediction and our experimental STM data nicely agree on the absolute numbers of enhanced rows as a function of the depth of Mn atom below the surface.

A transition from the "crablike" pattern[14] for Mn atoms in the topmost layer to a "bow-tie" shape[11] for deeply buried ones is of course expected. Up to now it has only been demonstrated for Mn in InAs (Ref. 28) but not for Mn in GaAs. These two materials significantly differ in a number of electronic properties, e.g., the bulk values of the band gap E_{gap}, the spin-orbit splitting of the valence band Δ_{SO}, and the binding energy of the Mn acceptor E_{Mn} bulk as reproduced from Ref. 29 in Table II. Obviously the band gap as well as the binding energy of manganese are much bigger in GaAs with respect to InAs, whereas the split-off energy due to spin-orbit coupling is quite similar in both materials. The binding energy of Mn in GaAs of 113 meV clearly points to a deep acceptor, whereas the value of 28 meV in InAs exactly equals the binding energy of Be in GaAs (Ref. 29) which is known as a clearly *shallow* impurity. Since shallow acceptors turned out to have a triangular contrast in STM on GaAs(110), whereas deep acceptors are characterized by bow-tie-shaped contrast, the contrast can be used to decide if an impurity is a deep or a shallow acceptor. However, the ratio of binding energy and band gap is rather similar for Mn in InAs and in GaAs. From this point of view, in spite of its small binding energy, Mn can still be seen as a *deep* acceptor

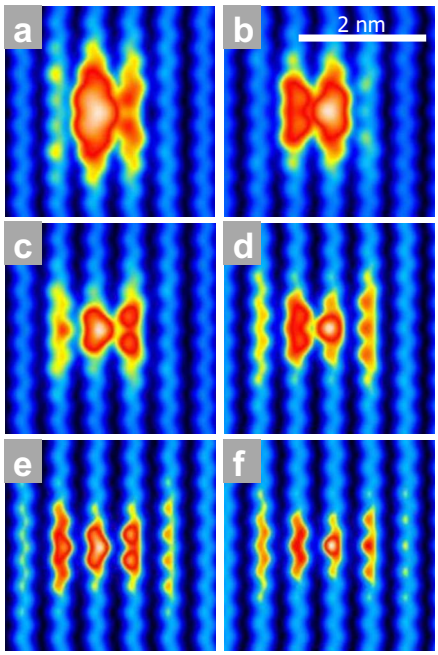

FIG. 4. (Color online) Simulated STM topography images taken from Ref. 14 of Mn acceptors in GaAs(110) in the surface [image (a)]. Frames (b)–(f) indicate Mn impurities which are each one atomic layer deeper below the surface. Note that the influence of the surface on the wave function is not taken into account. Bulk wave functions are integrated from E_F to +1.55 V and sliced in a (110) plane at the proper distance from the acceptor.

TABLE II. Comparison of electronic bulk properties of GaAs and InAs (Ref. 29).

	E_{gap} (eV)	Δ_{SO} (eV)	E_{Mn} (meV)	$E_{\mathrm{Mn}}/E_{\mathrm{gap}}$	$E_{\mathrm{Mn}}/\Delta_{\mathrm{SO}}$
GaAs	~1.5	0.34	113	~0.075	~0.66
InAs	~0.42	0.38	28	~0.067	~0.10

in InAs. Furthermore when tunneling on InAs with the metallic STM tip, the small band gap results in an accumulation layer of quasi-free-electrons in the tip induced quantum dot (TIQD) at the surface even at very low voltages,[30] which is not the case for GaAs. There the formation of a measurable TIQD requires a sample voltage of nearly −1 V.[31]

Due to these differences between InAs and GaAs, the Mn acceptor wave function cannot *a priori* be expected to have a similar shape at the surface and evolution toward the bulk in both materials. Mn acceptors in GaAs have been investigated directly in the surface[14] and several monolayers below,[11] but the transition region in between is still unknown. This connection is now resolved and allows us to compare Mn acceptors in different layers in the clearly different matrices GaAs and InAs with the following conclusion: none of the differences between InAs and GaAs strongly influences the contrast of the Mn acceptor. Following the general trend of shallow acceptors showing triangular patterns and deep acceptors being characterized by bow-tie-like shapes, Mn in InAs is a deep acceptor even though its binding energy equals only 28 meV. This is in contrast to the general classification of impurities given by Schubert,[32] which assigns a defect with a binding energy on the order of kT at room temperature and clearly smaller than 100 meV as shallow. Based on this, Mn is a deep acceptor in GaAs, whereas it falls in between shallow and deep in InAs. The same holds when one compares the experimentally observed binding energies with the values predicted by the EM approach. This approach results in 25.6 meV in GaAs and 16.6 meV in InAs. Thus the binding energy of Mn in GaAs is a factor 4.4 higher than the ideal EM acceptor, whereas this factor is only 1.7 for Mn in InAs. Furthermore, the wave function of EM impurities needs to be extended with respect to the lattice constant of the host material.

The influence of the TIQD is removed by the proper choice of the tunneling voltage and the tip induced band bending.[33] To map the ground state of Mn in GaAs one has to apply ~1.5 V, whereas only ~0.9 V is used to map the Mn ground state in InAs. According to Loth *et al.*[6] the GaAs(110) surface of *p*-doped material requires +1.56 V to reach the flat band condition, whereas this situation occurs at +1 V on *p*-doped InAs.[28] In both materials, the Mn ground state is thus mapped slightly below the flat band condition, where the depletion is small enough to allow tunneling current to pass, but no electron gas is present at the surface to screen the acceptor and thereby mask its contrast. After rescaling the acceptor binding energy with the band gap and thus interpreting Mn in InAs as a deep acceptor and applying the correct voltage to reach the same band bending situation at the surface, only the different spin-orbit splitting remains. Comparing Δ_{SO} with the binding energy for both materials, it turns out that the interaction with the split-off band is nearly a factor 5 smaller in InAs than in GaAs. The contrast of a magnetic impurity as Mn should be affected by the spin-orbit interaction; however the coupling between the acceptor state and the split-off band for Mn in GaAs has been shown to play a minor role.[19] Thus the smaller interaction hardly changes the Mn wave function in InAs with respect to Mn in GaAs.

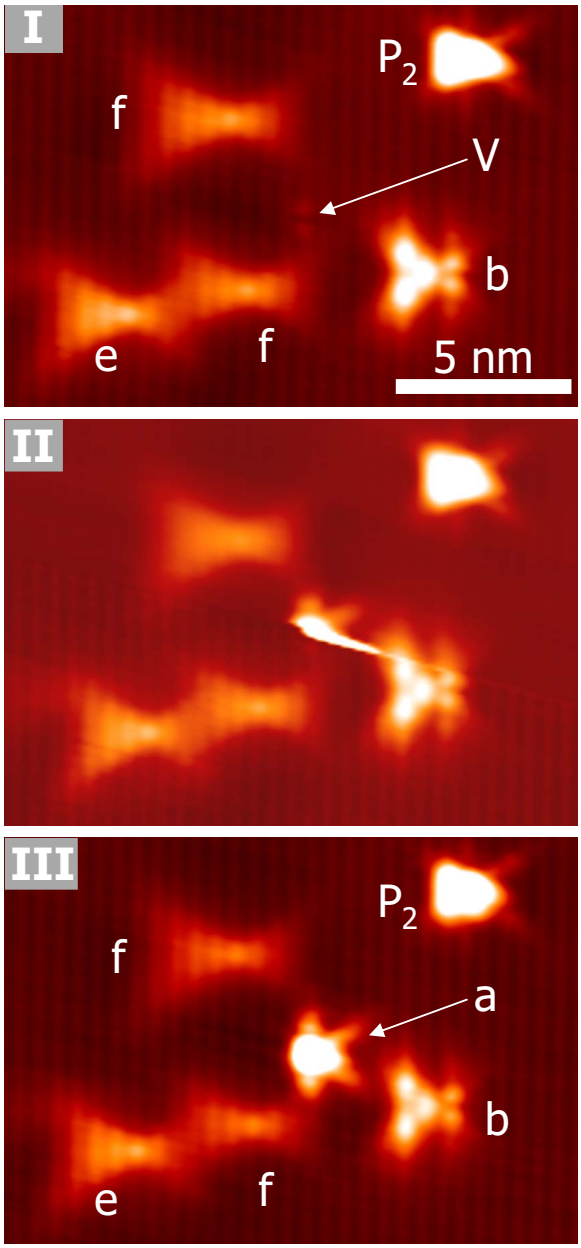

FIG. 5. (Color online) STM topography images on Mn doped GaAs(110) at 1.5 V, 50 pA, and 5 K sequentially taken on the same spot. Frame I shows five Mn-like features and one defect, most probably a surface vacancy. During frame II (scan direction pointing upward) an instability in the feedback loop occurred. Thereby a contrast similar to the one shown in Fig. 2(a) is created at the position of the vacancy. The stable final configuration is shown in frame III.

V. SURFACE MODIFICATIONS

Concerning pattern (a) we report the following interesting observation shown in Fig. 5. The topographic STM images I–III depicted in Fig. 5 were sequentially scanned with equal tunneling parameters of +1.5 V and 50 pA on the same spot of the Mn doped GaAs(110) surface. One Mn pair P_2, two deeply buried Mn atoms (f), and one Mn atom in each of layers 2 and 4 below the surface [patterns (b) and (e)] are

observed in image I. In addition there is another defect marked "V" with a rather weak contrast, which is probably a vacancy. In image II, which was scanned from bottom to top, the feedback loop shows an instability directly at the site of this weak contrast. The tip decreases in resolution but still keeps a reasonable imaging quality. Instead of the weak contrast V, the ongoing scan shows the upper half of a pattern that perfectly looks like feature (a) from Fig. 2 at the spot where V had been located. In the subsequently scanned frame shown in image III the tip even regains full atomic resolution confirming that V has been replaced by a contrast of type (a). To our opinion the contrast formed here does not differ from what has been identified as Mn in topmost surface layer of GaAs(110). In total we observed approximately ten of such tip induced contrast changes.

The explanation for the introduction of Mn-like features might be straightforward: the tip has picked up and then carried a Mn atom prior to the sequence shown in Fig. 5, where the Mn atom is released from the tip and inserted into the surface. For a single event, this mechanism would be satisfying. However we do not believe that this unlikely path gives a convincing explanation for an effect that appears more frequently. A better interpretation is based on the following: the differences between the transition metals Zn, Mn, Fe, and Co in the top layer of GaAs(110) in STM images as well as between Zn and Mn in the respective theoretical calculations[34] are rather small. This might stem from the fact that the atomic electronic structure of all of these elements ends with two electrons in the 4*s* shell. Pattern (a) in Fig. 2 then rather represents a quite general signature of transition metals (with two *s*-like valence electrons) in the GaAs(110) surface than really specific properties of individual chemical elements. As the electronic configuration of a big majority of the transition metals provides two *s*-like valence electrons, we have a wide choice of elements we probably inserted into the surface causing the contrast observed in image III of Fig. 5. The tip material W itself is the most natural species as it will of course be present at the tip apex. The electronic structure of W also terminates with two *s*-like valence electrons. The only difference of the atomic electronic structure of W with respect to the elements investigated in Ref. 34 is that they are bound in the 6*s* shell (for W) instead of the 4*s* shell for Mn, Fe, Co, and Zn. From the fact that Zn and Mn look completely different in STM if they are embedded deeper below the surface—Zn has a triangular, whereas Mn a bow-tie-shaped contrast—and appear very similar if they are substituted in the top layer, we conclude that the influence of the surface cannot be underestimated. This is stressed by the similar contrast of a Mn atom and a W atom in the topmost layer of GaAs(110) as W is not even known to behave as an acceptor up to now.

The possibility to easily insert a feature that looks like Mn, but most probably is not Mn itself, obviously increases the number of counts for type (a) with respect to the others as it is very unlikely to insert impurities with the STM into deeper layers. The total number of pattern (a) has thus been corrected for this effect. Another correction to the number of pattern (a) arises from the following observation concerning pattern P_2 which looks similar to a pair of Mn atoms on the next-nearest-neighbor positions on the Ga sublattice except

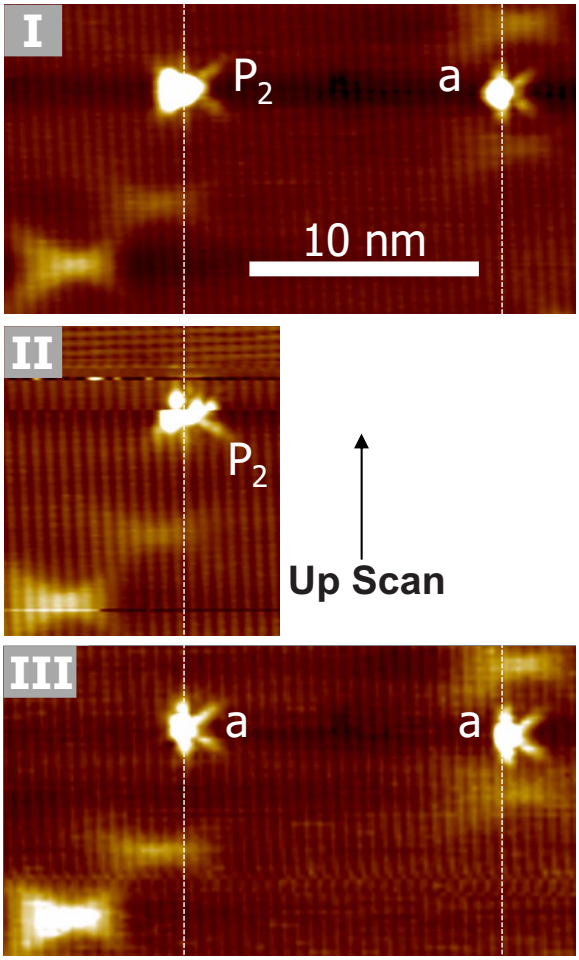

FIG. 6. (Color online) STM topography images sequentially scanned at 1.6 V and 50 pA on the same spot on GaAs(110). The feature P_2 in frame I is changed to pattern (a) as shown in Fig. 2 in frame III. Frame II shows the instability of the feedback loop directly occurring on P_2 connected to the modification. The white dashed lines show that the distance between the feature (a) on the right and the [001] end of the changing feature is constant. This confirms that the bigger protrusion of P_2 in $[00\bar{1}]$ direction is removed.

for the already mentioned asymmetry of pattern P_2 which is absent in the respective feature in Ref. 14 (see images II and IV of Fig. 3). One might thus explain the asymmetry of pattern P_2 as an unequal pair that consists of a Mn atom and an atomic impurity next to it instead of a pair of Mn atoms as investigated in Ref. 14. Pattern P_2 might also consist of a Mn atom with an adsorbate *on* the surface attached next to it. Figure 6 offers an answer to this question. It shows a sequence of STM images captured in constant current mode on the same spot on the cleavage surface. Image I shows one pattern P_2, one pattern (a), and two subsurface Mn atoms. While image II scanned an instability occurred on top of pattern P_2 clearly modifying it. The following image III confirms that a modification took place as pattern P_2 is replaced by pattern (a). From this observation we can draw two conclusions: first we identify the apex of the asymmetric protrusion of pattern P_2 that points in $[00\bar{1}]$ direction as the Mn

atom because it stays in the surface, whereas the wider part in $[00\bar{1}]$ direction of this feature is removed from the surface; second, the fact that no vacancy remains on the surface after removing the wider part of P_2 favors the interpretation of P_2 as an adsorbate bound to a surface Mn atom over the explanation as an unequal pair. As pattern P_2 has been found eight times in our measurements, it is remarkable that a complex of a Mn atom in the first layer with a rather undefined adsorbate atom gives rise to a reproducible contrast pattern. Unfortunately we do not have detailed knowledge about the chemistry of the adsorbate next to the Mn atom. In any case, Fig. 6 confirms the high reactivity of surface Mn atoms in GaAs(110).

Both the insertion of a transition-metal atom as well as the removal of an adsorbate bound to the surface Mn atom affect the number of the counts for pattern (a). On the one hand the number of inserted (a)-like features has to be subtracted, whereas on the other hand the pattern identified as P_2 stems from nothing more than masked single Mn atoms in the top layer and thus needs to be added to quantity (a). In total, both effects nearly cancel out. The corrected number of counts for (a) remains nearly unaffected (29 after the correction instead of originally 31).

Finally we want to address the role of temperature on these data. All images shown here have been acquired at 5 K, but additionally a similar set of measurements has been taken at 77 K. We did not count the defects in detail in the 77 K data, but concerning the topography we do not see a significant difference with the data measured at 5 K. It would even have been a surprise if the results strongly depended on temperature. The images just map the wave function of the acceptor states most probably convolved with the electronic structure of the buckled GaAs(110) surface. Except for thermal broadening, these properties are not expected to depend on temperature. This now leads to the question why these results have not been observed in earlier STM work on Mn doped GaAs at RT (e.g., the data behind Ref. 11). A simple explanation might be that the authors did not focus on the contrast of Mn in the top layer because it can easily be mixed up with adsorbates. A more involved interpretation is suggested on page 54 of Ref. 34; the STM was found to induce a reversed exchange process of a Co atom in the top layer which is kicked out of the surface and replaced by a Ga adatom. As we already mentioned, there are only minor differences between transition metals incorporated in the GaAs(110) surface. Even though the reverse incorporation is not reported for Mn, we still conclude that the reactivity of a surface unit cell containing a Mn atom is enhanced with respect to the undisturbed GaAs(110) surface. The rate and the mobility of atoms landing on the surface are enhanced at RT with respect to low temperature. Thus adsorbates typically get trapped at reactive sites on the surface and thus mask the Mn atoms in the topmost layer of GaAs(110). This mechanism prevents single Mn impurities in the topmost layer of the GaAs(110) surface from being observed at RT.

VI. CONCLUSIONS

In this work we experimentally identify buried Mn atoms in and below the GaAs(110) surface with monolayer precision. This connects the very recent results on Mn atoms inserted into the top layer of the surface by the STM tip with earlier measurements of buried Mn acceptors deeper below the surface. In addition we clearly injected defects which look very similar to Mn in the surface. As no Mn was present, we conclude that the contrast of an impurity—indeed if it is a transition-metal atom—is dominated by the electronic properties of the GaAs(110) surface rather than by the chemical nature of the impurity atom itself.

ACKNOWLEDGMENTS

We thank A. Yu Silov and M. Rohlfing for valuable discussions and the STW-VICI under Grant No. 6631, AS-PRINT, and FOM under Project No. 10001520 for financial support.

*j.k.garleff@tue.nl

[1] G. Binnig, H. Rohrer, Ch. Gerber, and E. Weibel, Appl. Phys. Lett. **40**, 178 (1982).
[2] G. Binnig, H. Rohrer, Ch. Gerber, and E. Weibel, Phys. Rev. Lett. **49**, 57 (1982).
[3] T. Trappmann, C. Sürgers, and H. v. Löhneysen, Europhys. Lett. **38**, 177 (1997).
[4] M. Schöck, C. Sürgers, and H. v. Löhneysen, Phys. Rev. B **61**, 7622 (2000).
[5] G. Mahieu, B. Grandidier, D. Deresmes, J. P. Nys, D. Stiévenard, and Ph. Ebert, Phys. Rev. Lett. **94**, 026407 (2005).
[6] S. Loth, M. Wenderoth, L. Winking, R. G. Ulbrich, S. Malzer, and G. H. Döhler, Phys. Rev. Lett. **96**, 066403 (2006).
[7] R. M. Feenstra, G. Meyer, F. Moresco, and K. H. Rieder, Phys. Rev. B **66**, 165204 (2002).
[8] T. Dietl, F. Matsukura, and H. Ohno, Phys. Rev. B **66**, 033203 (2002).
[9] T. Dietl, Semicond. Sci. Technol. **17**, 377 (2002).
[10] K. W. Edmonds, N. R. S. Farley, T. K. Johal, G. vanderLaan, R. P. Campion, B. L. Gallagher, and C. T. Foxon, Phys. Rev. B **71**, 064418 (2005).
[11] A. M. Yakunin, A. Y. Silov, P. M. Koenraad, J. H. Wolter, W. Van Roy, J. De Boeck, J.-M. Tang, and M. E. Flatté, Phys. Rev. Lett. **92**, 216806 (2004).
[12] A. M. Yakunin, A. Y. Silov, P. M. Koenraad, J.-M. Tang, M. E. Flatté, W. Van Roy, J. De Boeck, and J. H. Wolter, Phys. Rev. Lett. **95**, 256402 (2005).
[13] A. M. Yakunin, A. Y. Silov, P. M. Koenraad, J.-M. Tang, M. E. Flatté, J.-L. Primus, W. Van Roy, J. De Boeck, A. M. Monakhov, K. S. Romanov, I. E. Panaiotti, and N. S. Averkiev, Nat. Mater. **6**, 512 (2007).
[14] D. Kitchen, A. Richardella, J.-M. Tang, M. E. Flatté, and A. Yazdani, Nature (London) **442**, 436 (2006).
[15] J. K. Garleff, M. Wenderoth, R. G. Ulbrich, C. Sürgers, and H. v. Löhneysen, Phys. Rev. B **72**, 073406 (2005).
[16] J. K. Garleff, M. Wenderoth, R. G. Ulbrich, C. Sürgers, H. v.

Löhneysen, and M. Rohlfing, Phys. Rev. B **76**, 125322 (2007).
[17] A. P. Wijnheijmer, J. K. Garleff, P. M. Koenraad, K. Teichmann, M. Wenderoth, S. Loth, R. G. Ulbrich, M. Roy, and P. A. Maksym (unpublished).
[18] R. M. Feenstra, J. M. Woodall, and G. D. Pettit, Phys. Rev. Lett. **71**, 1176 (1993).
[19] C. Çelebi, P. M. Koenraad, A. Yu. Silov, W. Van Roy, A. M. Monakhov, J.-M. Tang, and M. E. Flatté, Phys. Rev. B **77**, 075328 (2008).
[20] C. Çelebi, J. K. Garleff, A. M. Yakunin, W. Van Roy, J.-M. Tang, M. E. Flatté, and P. M. Koenraad (unpublished).
[21] K. Sauthoff, M. Wenderoth, A. J. Heinrich, M. A. Rosentreter, K. J. Engel, T. C. G. Reusch, and R. G. Ulbrich, Phys. Rev. B **60**, 4789 (1999).
[22] J. K. Garleff, M. Wenderoth, K. Sauthoff, R. G. Ulbrich, and M. Rohlfing, Phys. Rev. B **70**, 245424 (2004).
[23] K. Besocke and H. Wagner, Phys. Rev. B **8**, 4597 (1973).
[24] P. Hahn, J. Clabes, and M. Henzler, J. Appl. Phys. **51**, 2079 (1980).
[25] M. A. Rosentreter, M. Wenderoth, N. H. Theuerkauf, A. J. Heinrich, M. A. Schneider, and R. G. Ulbrich, Phys. Rev. B **56**, 10538 (1997).
[26] J. M. Sullivan, G. I. Boishin, L. J. Whitman, A. T. Hanbicki, B. T. Jonker, and S. C. Erwin, Phys. Rev. B **68**, 235324 (2003).
[27] A. Stroppa, X. Duan, M. Peressi, D. Furlanetto, and S. Modesti, Phys. Rev. B **75**, 195335 (2007).
[28] F. Marczinowski, J. Wiebe, J.-M. Tang, M. E. Flatté, F. Meier, M. Morgenstern, and R. Wiesendanger, Phys. Rev. Lett. **99**, 157202 (2007); S. Loth, M. Wenderoth, and R. G. Ulbrich, Phys. Rev. B **77**, 115344 (2008).
[29] O. Madelung, *Semiconductors-Basic Data*, 3rd ed. (Springer, New York, 2004).
[30] R. Dombrowski, Chr. Steinebach, Chr. Wittneven, M. Morgenstern, and R. Wiesendanger, Phys. Rev. B **59**, 8043 (1999).
[31] M. Wenderoth, M. A. Rosentreter, K. J. Engel, A. J. Heinrich, M. A. Schneider, and R. G. Ulbrich, Europhys. Lett. **45**, 579 (1999).
[32] E. F. Schubert, *Doping in III-V Semiconductors* (Cambridge University Press, Cambridge, England, 1993).
[33] R. M. Feenstra and J. A. Stroscio, J. Vac. Sci. Technol. B **5**, 923 (1987).
[34] D. Kitchen, Ph.D. thesis, Urbana-Champaign, 2005.